Photochromism of doped terbium gallium garnet

H. Dachraoui,[1] R. A. Rupp,[1] K. Lengyel,[2] M. A. Ellabban,[1] M. Fally,[1] G. Corradi,[2] L. Kovács,[2] and L. Ackermann[3]

[1]*Faculty of Physics, Nonlinear Physics Group, Universität Wien, Boltzmanngasse 5, A-1090 Wien, Austria[*]*
[2]*Research Institute of Solid State Physics and Optics, Hungarian Academy of Sciences, Konkoly-Thege M. út 29-33,*
H-1121 Budapest, Hungary
[3]*Forschungsinstitut für Mineralische und Metallische Werkstoffe, D-55743 Idar-Oberstein, Germany*
(Received 21 July 2006; published 18 October 2006)

In order to understand the photochromic effect in terbium gallium garnet doubly doped with calcium and cerium, the spectral characteristics of absorption changes induced by heating and irradiation are studied. Based on the findings we conclude that the photochromic band at 420 nm originates from defects involving Tb^{4+}. Previously the band was attributed to Ce^{3+}. Two possible models are suggested and discussed, both of which are in agreement with the obtained experimental results.

I. INTRODUCTION

Terbium gallium garnet crystals (TGG, $Tb_3Ga_5O_{12}$) combine relatively high Verdet constant,[1,2] low absorption coefficient, and high thermal conductivity.[3] Moreover, it is commercially available with high optical quality. Therefore, it is preferred over other magneto-optic materials at high-power applications for constructing efficient optical rotators and isolators. Furthermore, it can be used for substrates and waveguides in combination with other garnets as its lattice constants can be adjusted over a wide range using different rare-earth ions.[4]

TGG has a cubic crystal structure of point group symmetry $m\bar{3}m$. Hence, odd-rank tensors vanish and the standard photorefractive effect based on the Pockels effect is not possible. Nevertheless, light-induced refractive-index changes have been confirmed by two-wave mixing experiments.[5] In order to find a microscopic explanation for this photorefractive effect, the first step is to identify the photochromic bands that are connected with these changes of the refractive index by the Kramers-Kronig relations. The photorefractive effect is particularly pronounced in TGG samples, which exhibit a characteristic photochromic band approximately centered at the wavelength $\lambda = 420$ nm that occurs in samples doubly doped with calcium and cerium. According to Reyher *et al.*,[6] results obtained from optically detected magnetic resonance (ODMR) and magnetic circular dichroism (MCD) seem to suggest that Ce^{3+} ions in connection with other unidentified charge carrier traps are responsible for the photorefractive effect in TGG.

In this work we present findings from a detailed absorption spectroscopic study that contradict the interpretation of Reyher *et al.* and thus compel us to propose a different model for the photochromism in TGG:(Ca, Ce).

II. EXPERIMENTS

The samples were taken from boules grown by the Czochralski technique for the fabrication of optical isolators. In order to stabilize the growth of boules of large diameter, some calcium is added to the melt, causing an undesirable coloration that has been attributed to the generation of color centers in a similar garnet.[7] Adding cerium suppresses this coloration. The effect is believed to be due to charge compensation.[6,8] The samples have cylindrical shape with a radius of 2.5 mm and various thicknesses d. The polished end-faces are perpendicular to the crystallographic [111] direction. Table I gives an overview of the investigated samples.

Absorption spectra for the UV and visible spectral range were recorded with the spectrometers CARY5G (Varian) and V-550 (Jasco). In order to induce photochromic changes at well-defined wavelengths in reasonable time, an Argon ion ($\lambda = 458$, 476, 488, 501, and 514 nm), a frequency-doubled Nd:yttrium aluminum garnet (YAG) ($\lambda = 532$ nm), or a helium-neon ($\lambda = 632.8$ nm) laser were used as irradiation sources, respectively.

On all the following graphs either the optical density (absorbance) is given or the absorption coefficient α. In the latter case the data have been corrected for reflection. Where

TABLE I. Investigated samples. Concentrations refer to the ratio of the dopant added to the melt. For sample T8, the presence of dopants is known but not their quantities.

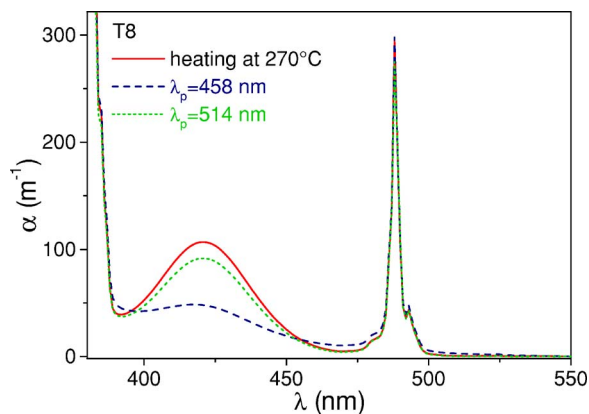| Sample	Doping wt (ppm)		Doping mol (ppm)		Color	Thickness (mm)
	Ca	Ce	Ca	Ce		
T5.2	25	25	640	180	Yellowish	0.38
T6	25	65	640	470	Yellowish	2.02
T8	×	×	×	×	Yellowish	14.50

144104-1

FIG. 1. (Color online) Absorption spectra for sample T8 at room temperature after illumination with either λ_p=458 or 514 nm or heating for 1 h at 270 °C.

we report absorption differences the reflection correction does not matter. Thermal relaxation was monitored while the sample was kept at constant temperature in an oven inserted into the spectrometer.

Since the absorption band at λ=420 nm is sufficiently broad, we monitored its photo-induced kinetics with a light-emitting diode (LED) emitting at λ=410 nm. The intensity was measured by a photodiode behind the output face. Thereby the actinic light that induces the photochromic changes was blocked off by an interference filter.

III. EXPERIMENTAL RESULTS

In Sec. III A basic facts on the photochromism of TGG are reviewed. Section III B presents the spectral investigations of the kinetics.

A. General features

Figure 1 displays the spectra for sample T8 obtained after sufficiently long irradiation with linearly polarized actinic light at λ_p=458 nm and λ_p=514 nm, respectively, in comparison to the spectrum after sufficiently long annealing at elevated temperature [the subscript p (pump) refers to actinic irradiation]. Besides the strong increase of absorption toward the UV one recognizes the sharp peak of the characteristic transition $^7F_6 \rightarrow {}^5D_4$ of Tb^{3+} at about 488 nm that, as an electric dipole transition of the free ion, would be spin-forbidden. In between there is a well-resolved broader band, the prominent photochromic band at 420 nm. This band is denoted by B.42, and analogous notations will be used for all further photochromic bands. B.42 will be used as the reference and monitor for changes of the state of the sample.

In practice B.42 was monitored by recording the transmitted intensity I_t at λ_r=410 nm [the subscript r (read-out) refers to the monitoring light]. Thus, at a chosen intensity I_p and wavelength λ_p of the actinic light the transmission of the samples was studied as a function of the time t elapsed since the beginning of irradiation. Different curves were obtained providing the evidence that the kinetics becomes faster with increasing intensity I_p (kept constant during a run). If we
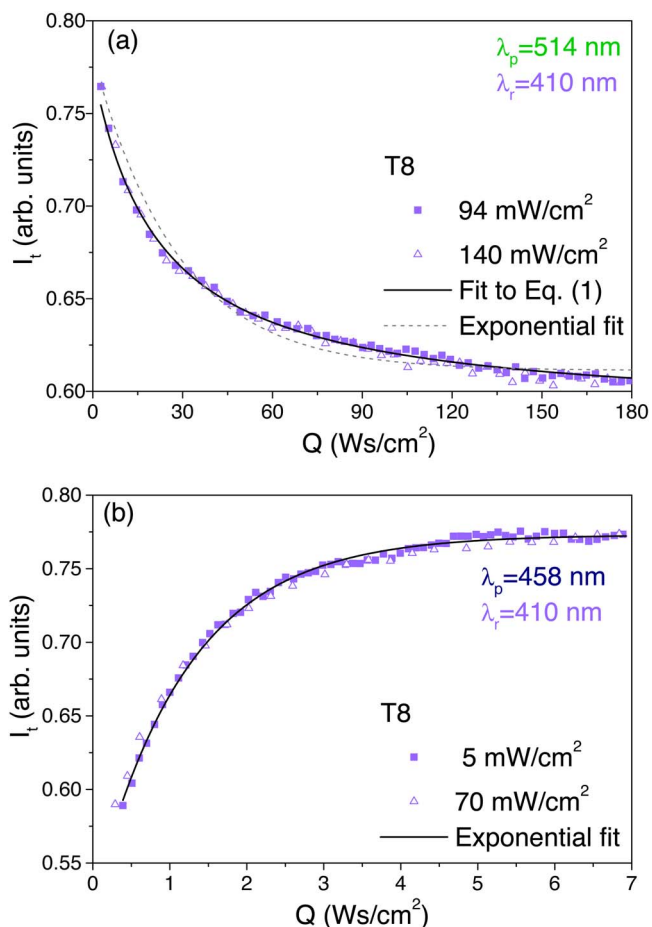

FIG. 2. (Color online) Transmitted intensity of sample T8 as a function of exposure ($Q=I_p t$) for two different intensities at (a) λ_p=514 nm and (b) 458 nm, monitored at λ_r=410 nm. Solid lines are fits to Eq. (1) and an exponential decay, respectively.

plot, however, the transmitted intensity I_t as a function of the exposure variable $Q=I_p t$, all data are on the same universal curve. In Fig. 2 some examples are given. Figure 2(a) shows the data of the kinetics at λ_p=514 nm for the intensities I_p=94 mW/cm^2 and I_p=140 mW/cm^2, respectively. More striking is Fig. 2(b) at λ_p=458 nm, where the actinic intensities with I_p=5 mW/cm^2 and I_p=70 mW/cm^2 differ even by more than one order of magnitude.

Upon prolonged irradiation the transmission is asymptotically striving toward a limiting value. After many experiments varying the treatment of the sample prior to exposure, we came to the conclusion that the coloration of the sample for $Q \rightarrow \infty$ does not depend on the initial state of the sample. Henceforth we refer to this limiting case as the stationary state of the sample for λ_p. As for Fig. 1, we can now precisely define what we mean by "sufficiently long irradiation," namely, a time span large enough to approach the characteristic final spectrum with sufficient accuracy.

In our experiments the lowest stationary absorbance for B.42 resulted from irradiation at λ_p=458 nm. Later arguments will make it quite plausible that irradiation at the central wavelength of the band would have resulted in further decrease of absorbance, but since no sufficiently strong irradiation source at λ_p=420 nm was available to us that would

TABLE II. Saturation absorption change $\Delta\alpha(t=\infty)$ of the band B.42 achieved by irradiation at different pump wavelengths.

λ_p (nm)	476	488	496	501	514	532	633
$\Delta\alpha$ (cm^{-1})	7.9	14.2	15.6	15.5	18.6	16.1	6.6

have permitted us to reach the stationarystate within reasonable time, we take in the following the stationary state at $\lambda_p=458$ nm, with the characteristic spectrum shown in Fig. 1 as a reference state, and call it the *bleached* state.

In order to characterize the photoinduced coloration of band B.42 as a function of the wavelength λ_p of the actinic radiation, we first transferred the sample to the bleached state by irradiation with $\lambda_p=458$ nm. Then the sample was irradiated with any of the available wavelengths until steady state. The absorption difference $\Delta\alpha(Q=\infty)$ between this steady state and the bleached state was measured at $\lambda_r=410$ nm. Results for sample T8 are given in Table II. The most pronounced coloration is found if the crystal is irradiated in the wavelength range 488–532 nm, albeit there is still significant coloration at 477 nm and 633 nm.

As a typical example for the spectra resulting from irradiation at other wavelengths, the one obtained by irradiation with green light is displayed in Fig. 1. Correcting for background its band B.42 can be estimated to be about 2.1 times as large than the one of the bleached state. A unique stationary state is also approached for prolonged annealing at sufficiently elevated temperatures. The absorption coefficient at 420 nm is about 2.7 times larger than the one of the bleached state. Since the thermally induced stationary state gives a larger absorbance than could be reached by irradiation at any of the wavelengths investigated, we take this as a second reference state and call it the *fully colored* state.

As TGG is cubic, one would not expect any significant optical anisotropy. Nevertheless, an inspection along the [111] axis of the sample T8 was performed under orthoscopic observation conditions between crossed polarizers. It revealed a periodic change of the transmitted intensity when rotating the sample around its cylindrical axis. This can be attributed to presence of a weak ($<10^{-6}$) birefringence distinguishing two main axes of polarization for beam propagation along the [111] axis. Therefore we compared the case of an irradiation with a polarization parallel to one of the main axes ($\theta=0°$) with the case of irradiation with a polarization at 45° with respect to the main axes ($\theta=45°$). From Fig. 3 it can be seen that only a negligible dependence on polarization is found for the coloring wavelengths $\lambda_p=514$ nm and 633 nm, which can be neglected in first approximation. In contrast, there is a pronounced dependence on the polarization for irradiation at the bleaching wavelength $\lambda_p=458$ nm. The most efficient bleaching is found for a polarization along one of the main axis directions of the sample.

So far, we may summarize our findings by stating that for a given photon energy and polarization of the actinic light, the same stationary spectrum is achieved in the limit $Q \rightarrow\infty$, regardless of the initial state of the sample. Further, it is our experience that any state to which the sample had been transferred to can be considered as practically frozen in at room temperature. On the other hand, annealing at sufficiently high temperature transfers the sample to the fully colored state. In Fig. 4 we study therefore the thermally induced transition from the bleached state at room temperature to the colored state. To that purpose we measure the absorption coefficient α at $\lambda_r=410$ nm as a function of temperature. Heating was performed at a rate of approximately 9 K/min. Up to 150 °C the absorbance increases only slightly. Beyond that temperature a strong rise of absorption sets in that is particularly dramatic above about 200 °C. Particularly important is the point that the absorbance change proves to be thermally irreversible. Cooling from the colored state at 295 °C at a rate of approximately 3 K/min leads to a col-
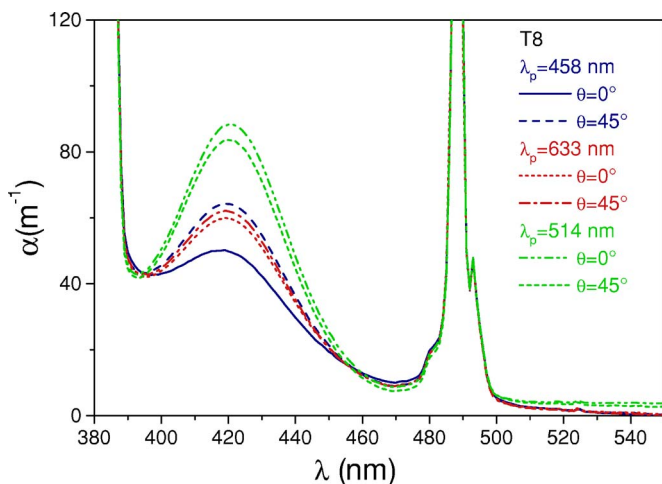

FIG. 3. (Color online) Absorption spectra of sample T8 for different polarization states and wavelengths of the pump beam.
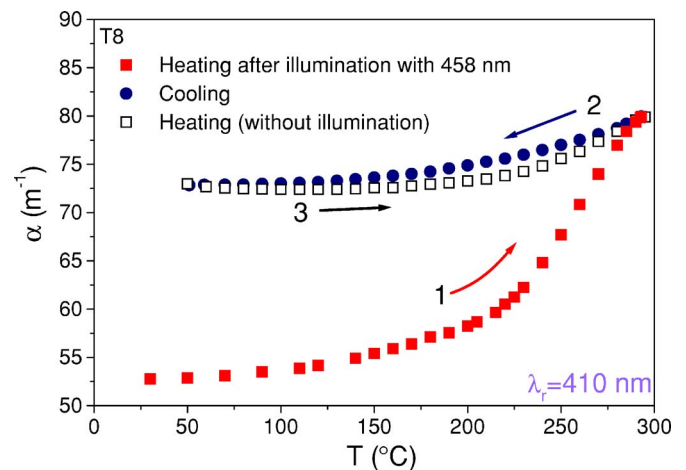

FIG. 4. (Color online) The absorption coefficient for sample T8 at $\lambda_r=410$ nm upon temperature cycling 1-2-3 starting from the bleached state.
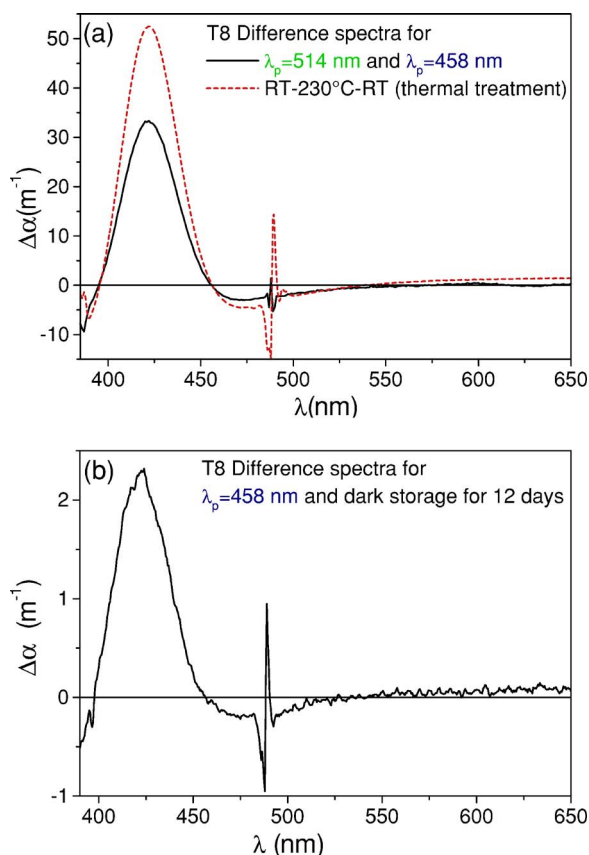
FIG. 5. (Color online) Differences of absorption spectra of sample T8. In all cases the spectrum of the bleached state resulting from irradiation at 458 nm is subtracted. (a) Difference spectra for a sample irradiated at 514 nm (full line) and for a sample annealed at 230 °C (dashed line). (b) Difference spectrum resulting from dark storage for 12 days at room temperature.

ored state at 50 °C that drastically differs from the original bleached state. The latter thermal path is completely reversible, i.e., the fully colored state can be regarded as thermally stable. (The fact that we stopped cooling at 50 °C is caused by the diverging cooling time, and the slight hysteresis in Fig. 4 has its reasons in the experimental apparatus.)

Figure 5 compares difference spectra at room temperature with respect to the bleached state. In Fig. 5(a) spectra were taken after irradiation with 300 W s/cm^2 at 514 nm (full line) and after annealing at 230 °C (dashed line), and in both cases the reference spectrum taken after irradiation with 80 W s/cm^2 at 458 nm was subtracted. First of all we note that apart from the height both spectra look roughly the same, taking into account that the striking difference at the position of the sharp peak at 488 nm could be attributed to an instrumental artefact. The higher sensitivity of the difference spectra with respect to photochromic changes permits clear identification of an additional photochromic band B.49 at about 490 nm. Since its oscillatory strength is only 10% of B.42, it escaped notice in former studies. The band shape of B.49 is not symmetric with respect to the center of the peak. This can be attributed to overlap with the stronger band B.42. Furthermore, the spectra of sample T8 provide first hints for photochromic changes in the UV and in the far red that will be explored later on.

In order to answer the question as to whether the bleached state is a thermodynamically stable state at room temperature or only a metastable state that is kinetically frozen in at room temperature, the following experiment was performed: Sample T8 was first transferred to the bleached state by irradiation with 25 W s/cm^2 at 458 nm. Immediately afterward a spectrum was taken that serves as the reference spectrum. Then the sample was kept in the dark for 12 days, after which a second spectrum was taken from which the reference spectrum was subtracted. The resulting difference spectrum is shown in Fig. 5(b). Although much weaker, we see again the same characteristic spectroscopic fingerprint of the photochromic changes like in Fig. 5(a). Hence, temperature determines only the decay time with which the bleached state relaxes back toward the colored state. At room temperature this relaxation is very slow but obviously present.

As a conclusion we may draw the following preliminary picture: Irradiation into the band B.42 causes a photoinduced transition to a metastable nonequilibrium state, the bleached state. This state relaxes back into the the colored state, being the equilibrium state, either by thermally induced processes or by irradiation at longer wavelengths. The relaxation time of thermally induced processes strongly depends on temperature.

B. Thermal relaxation kinetics

The experimental facts presented so far suggest the following investigation procedure: First the sample is brought into the bleached state by irradiation with $\lambda_p = 458$ nm. Then the sample is inserted into the photospectrometer and rapidly heated to a selected annealing temperature at which the initial spectrum is taken at a time t_0. Finally, spectra are taken at some later time t to follow the thermally induced coloration kinetics. By plotting the difference spectra with respect to the one at initial time t_0, i.e., the spectra of the absorbance change $\Delta A(t) = A(t+t_0) - A(t_0)$, we may take advantage of the high reliability to detect even small absorption changes since the sample is not removed from the sample chamber between the measurements.

Apart from the decay kinetics, the spectra of sample T8 obtained at annealing temperatures between 200 °C and 250 °C are not much different. Therefore it is sufficient to display one example, and we have chosen the spectrum for sample T8 at $T = 210$ °C shown in Fig. 6. Five distinct structures can be seen in the difference spectrum: (i) a decreasing absorbance region extending toward the ultraviolet from which only the edge is seen within the spectral range investigated [B.31–B.36, these UV bands at 310 and 360 nm and their evolution are clearly observed in the thin sample T5.2, see Figs. 7(a) and 7(b)]; (ii) the well-known increasing broad band centered at 420 nm (B.42); (iii) a decreasing broad band centered at about 490 nm (B.49); (iv) the superposed narrow structure at 488 nm which resembles the derivative of an absorption band; and (v) an increasing very broad absorption range extending into the near-infrared region (B.75).

It is obvious that the derivative-like absorption structure points to a slight shift of the position of the $^7F_6 \rightarrow {}^5D_4$ transition of Tb^{3+}, but since we have not investigated it thor-
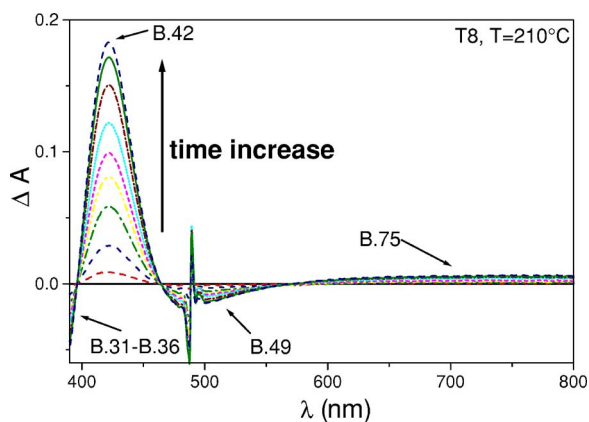
FIG. 6. (Color online) Change of the absorbance-difference spectra at various time intervals for sample T8 at constant temperature $T=210\,°C$.

oughly enough and hence cannot completely rule out the possibility of an instrument-generated artefact, we will not consider it any further. We will focus our discussion on the broad spectral changes only.

The absorption change extending to the UV, only adumbrated in Fig. 6, was explored down to 300 nm by using a thinner sample, T5.2. Absorbance spectrum and difference spectrum are shown in Fig. 7. We recognize a decreasing broad, very strong absorption range which seems to be made up of two overlapping bands centered at approximately
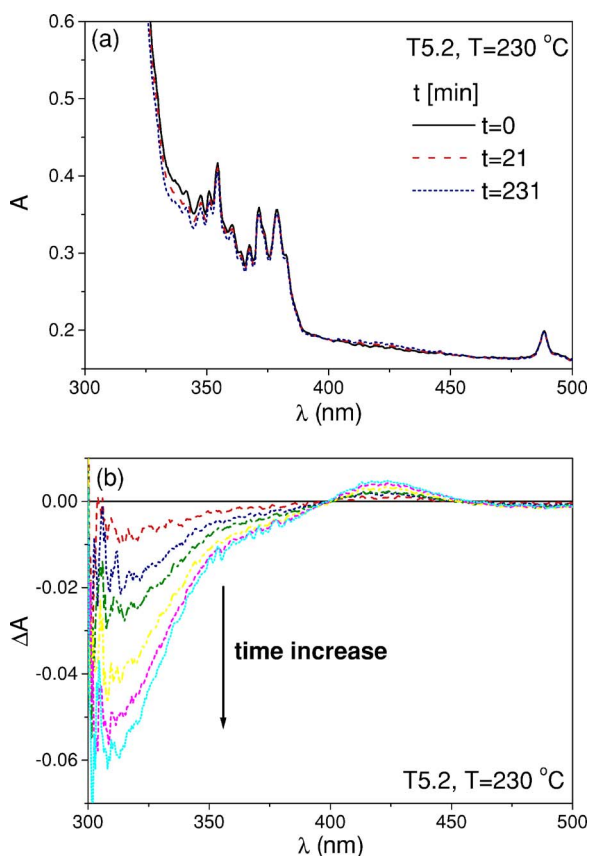

FIG. 7. (Color online) Spectra for (a) absorbance and (b) absorbance changes in sample T5.2 at constant temperature $T=230\,°C$.

TABLE III. Overview on approximate positions, relative heights, and bandwidths, full width at half maximum (FWHM), of the photochromic bands detected in TGG:(Ca,Ce). A positive sign means increase of the band upon thermal annealing.

Band notation	Position of maximum (nm)	Sign of thermally induced change	Relative height of maximum	FWHM (eV)
B.31	310	−	12	0.8
B.36	380	−	2	0.5
B.42	420	+	1.0	0.3
B.49	490	−	0.1	0.3
B.75	>700	±	0.02	≈1

310 nm and 380 nm, respectively. The latter is only indicated as a shoulder of the band at 310 nm.

Table III summarizes the characteristics of the five photochromic bands observable in TGG:(Ca, Ce).

The heights of the maxima extend over nearly three orders of magnitude, and even the integrated absorption of the bands ranges over approximately two orders of magnitudes. Also the full widths of half maximum (FWHM) are given. From the data it was not possible to deduce the width of the extremely broad band B.75 easily, so that we may only roughly estimate it to be in the range of 1 eV.

Each difference spectrum exhibits three points where the thermally induced absorption change vanishes. A magnified view of these crossover regions for the bands B.36/B.31–B.42 and B.42–B.49 can be seen in Fig. 8(a). The points of zero absorption are identical for all curves and are thus isosbestic points. They are situated at $\lambda_{i1}=397$ nm and $\lambda_{i2}=463$ nm. In the room temperature spectra [e.g., Fig. 5(a)] there are also two isosbestic points but somewhat shifted toward lower wavelengths: $\lambda_{i1}=395$ nm and $\lambda_{i2}=455$ nm. The situation at the crossover between the bands B.49 and B.75, shown in Fig. 9, is different. Here the point of zero absorption change shifts by more than 30 nm with increasing time of relaxation.

A comparison of the spectra of the absorbance difference for samples T6 and T8 with respect to the bleached and colored state reveals essentially the same bands. An example for sample T6 is shown in Fig. 10 at an annealing temperature of 250 °C. The only difference with sample T8 is that the sign of the thermally induced absorption change for B.75 is negative.

Finally, let us recall that all quantitative investigations of the kinetics started from the same initial conditions. At first the samples were irradiated at $\lambda_p=458$ nm with the same exposure of 40 W s/cm^2. Then the spectrum of the bleached state at room temperature was taken. Subsequently the samples were heated to the target temperature and the relaxation to the colored state was followed as a function of time, usually for more than 3 h, giving a series of difference spectra as shown in Fig. 8(a) for sample T8 at 230 °C. Then the absorbance between the two isosbestic points of B.42 was integrated and plotted as a function of time. An example is shown in Fig. 8(b). In all cases investigated there was a clear discrepancy between the data and a best fit according to the
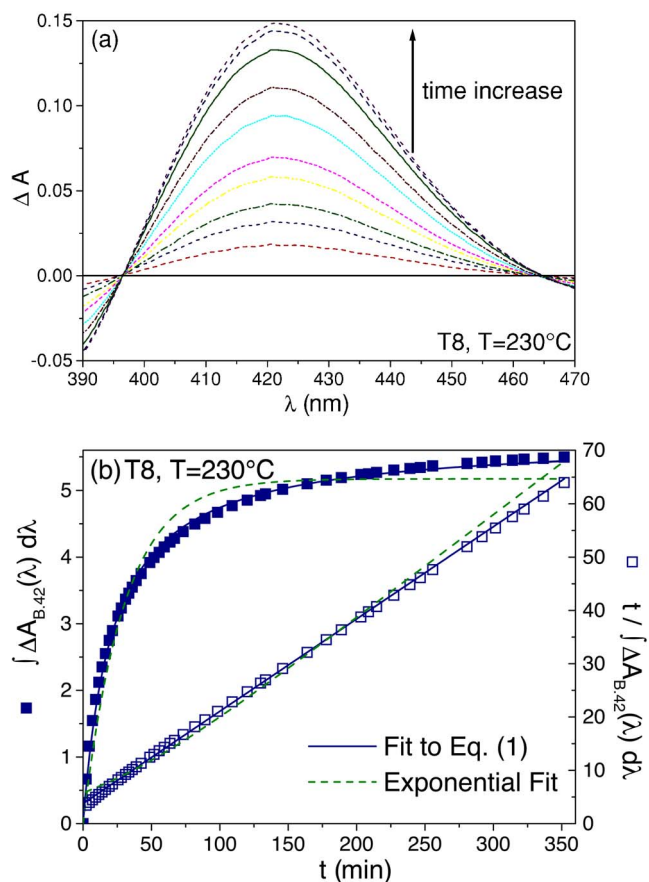
FIG. 8. (Color online) (a) Difference spectra of absorbance for sample T8 at $T=230\,^{\circ}\text{C}$ and (b) the kinetics of the band B.42 deduced by integration of the absorbance change between the isosbestic points. The solid line represents a fit to Eq. (1).

exponential relaxation model $\Delta A(t) = \Delta A(\infty)[1 - \exp(t/\tau)]$, where τ represents the relaxation time constant.

In contrast, the kinetics of absorbance for B.42 can satisfactorily be described for sample T8 as well as for sample T5.2 by the function
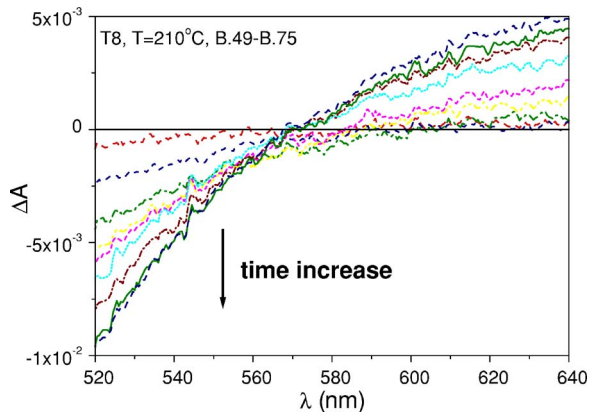

FIG. 9. (Color online) Magnified view in the region of vanishing absorption change for sample T8 at $T=210\,^{\circ}\text{C}$ between the bands B.75 and B.49.
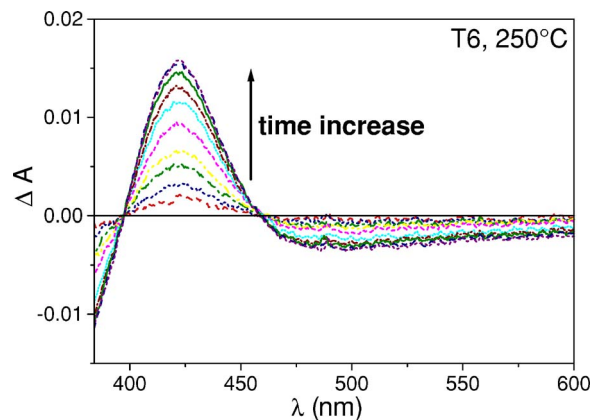

FIG. 10. (Color online) Spectra of absorbance differences between bleached and colored state for sample T6 at $T=250\,^{\circ}\text{C}$.

$$\Delta A(t) = \Delta A(\infty)\frac{t}{t + \tau}. \tag{1}$$

It is quite instructive to plot the variable $t/\Delta A(t)$ as a function of t. Then for all cases investigated the data points are always on a straight line, as shown on the right scale of Fig. 8(b), and we obtain $1/\Delta A(\infty)$ from the slope and $\tau/\Delta A(\infty)$ from the intercept.

For both samples the temperature dependence of the time constants determined in that way follows in good approximation an Arrhenius law with $\tau \propto \exp(-E_A/k_B T)$, where E_A is the activation energy and $k_B T$ the thermal energy. Because of the narrow temperature interval between $200\,^{\circ}\text{C}$ and $250\,^{\circ}\text{C}$ explored in our investigations and scattering of our data, the activation energy E_A for both samples can only be roughly estimated to be between 0.6 and 1.4 eV.

IV. DISCUSSION

First we will discuss the possible states of absorption induced by heating or illuminating TGG:(Ca,Ce) at different wavelengths, then analyze the different induced absorption bands, and finally we will discuss two models for candidate centers of the band that can explain the photochromic effect in TGG:(Ca,Ce) samples consistently with the experimental results.

The characteristic absorption spectra for TGG:(Ca,Ce) samples as depicted in Fig. 1 clearly distinguish two absorption states: the bleached state and the fully colored state. Bleaching can be reached by irradiating the sample with light in the blue spectral range, whereas coloring is obtained by illumination in the green, or even more effective, by annealing at elevated temperatures. The photoinduced kinetics measured at different intensities of the green and the blue light as shown in Fig. 2 follow a universal curve, which depends only on the exposure $Q=I_p t$ (i.e., on the number of absorbed photons and not on the intensity of the photon field). From the measurements presented in Fig. 4 we infer that the colored state (induced by heating) is the thermodynamically stable one, whereas the bleached one has to be regarded as a metastable state of the sample. This conclusion is supported

by the observed ultraslow relaxation shown in Fig. 5(a). Keeping the sample in the dark for two weeks, the bleached state shows a small but nevertheless perceptible reduction of about 3%. The population of the metastable state strongly depends on the wavelength of the pump light, as can be seen in Fig. 3. Thus, the strong photochromic effect in TGG can be attributed to the existence and metastability of this state.

All sharp features in the spectra (330–380 nm and near 488 nm) can be attributed to bulk Tb^{3+} as discussed already by Reyher *et al.*[6] and references therein. In particular, we may identify the *f-f* transitions from the $^7F_6$ ground state to the $^5D_4$ manifold at 488 nm and to the series of sharp transitions starting with $^5D_3$ at about 380 nm. As a rule, these features are small in the difference spectra [Figs. 5, 6, and 7(b)] or even absent as in the case of the 488 nm feature for sample T6 [Fig. 10]. These Tb^{3+} bands do not overlap the isosbestic points at $\lambda_{i1}=396$ nm and $\lambda_{i2}=464$ nm [Fig. 9(a)] and do not seem to be involved in the transformations governing the intensity changes of the photorefractive band at 420 nm. This is not surprising for the following reason: All photochromic bands are clearly defect-related bands since they do not occur in nominally pure samples. Hence they result from changes in the order of the defect concentration that is below 0.01 mol % for the Ca and/or Ce doping of our samples, but changes of any band of the host crystal below 10^{-4} are not resolvable by our measurement technique. So even if Tb^{3+} would take part in the photochromic reaction, its involvement could not be detected from a change of bands of the host material, e.g., of the sharp band at 488 nm.

The defect-induced broad bands B.31/B.36, B.42, and B.49 are closely related. This can be verified by plotting the absorbance changes of the bands with respect to each other for all annealing times. As an example, the absorbance changes of band B.42 vs that of B.31/B.36 is plotted in Fig. 11(a) for all annealing times. Straight lines, i.e., strictly linear relationships, are found. This means that the underlying states are clearly transferred into each other by exactly the same kinetics. Further confirmation comes from the fact that two isosbestic points at $\lambda_{i1}=397$ nm and $\lambda_{i2}=463$ nm can unambiguously be identified for all irradiation-induced processes as well as for thermal relaxation processes, as shown in Figs. 5(a) and 8(a), respectively. This means that the relaxation process is in first approximation a reaction of the simple type $B_1+B_2+\cdots \rightleftharpoons C_1+C_2+\cdots$ between centers pertinent to the bleached (B) and the colored (C) state. The bands B.31, B.35, and B.49 have to be attributed, therefore, to one or more of the centers B_i and the band B.42 to one of the centers C_i.

The defect-related band B.75 behaves quite different and has to be distinguished from the bands just discussed. We attribute it to a different center P. There is no isosbestic point between B.49 and B.75, as can be seen from Fig. 9. Further, there is no linear dependence of B.75 on B.42 [Fig. 11(b)], i.e., the B and C defects on the one hand and the defect P contributing to B.75 on the other hand follow a strikingly different kinetics. We anticipate that given the large width of B.75, polarons are the most plausible centers responsible for the occurrence of band B.75. Since P has no apparent influence on the isosbestic points at $\lambda_{i1}=397$ nm and $\lambda_{i2}=463$, the center is either decoupled from the reaction between B_i
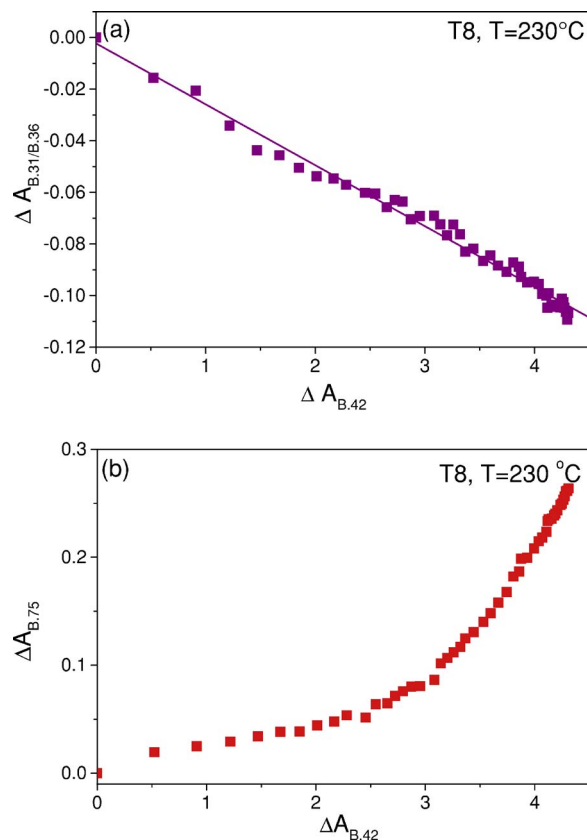

FIG. 11. (Color online) Absorbance change of (a) the band B.31/B.36 and (b) the band B.75 as a function of the absorbance change of the band B.42 for the sample T8 at 230 °C in arbitrary units.

and C_i or it is involved, but contributes with a concentration that is negligible to the ones of B and C. The latter would imply that the oscillatory strength of center P is strong.

Reyher *et al.* assigned the band B.42 to Ce^{3+} on the basis of the MCD spectra of their undoped and Ca/Ce codoped TGG samples, and explained the corresponding ODMR band by comparing the observed *g* factor with other Ce^{3+} data.[6] However, if band B.42 is assigned to Ce^{3+}, then it is expected that the strength of the band increases as the concentration of Ce increases. In contrast, we found that the band decreases with higher Ce concentration. If we compare the saturation absorption change of band B.42 normalized by the thickness d (i.e., $(1/d)\int \Delta A d\lambda$, integrated between the isosbestic points), for the samples T5.2 (25 ppm Ce) and T6 (65 ppm Ce), then the ratio is 0.64. Since the Ca doping of 25 ppm is the same in both samples we are confronted with the fact that increasing the Ce ratio by a factor 2.6 does not increase the band B.42, but on the contrary, reduces it by a factor 1.7. Thus we reject the assumption of Ce^{3+} being responsible for the band at 420 nm and have to look for other possibilities.

First we discuss the role of calcium. It is added to the melt in order to facilitate the growth of single crystals with excellent optical quality. However, in those garnets where earth alkali ions replace three valent host ions there is a heavy price to pay. Because of the charge neutrality condition oxygen vacancies and different types of pertinent color centers are generated.[9] In the particular case of TGG there is the

TABLE IV. Charge-transfer bands of Tb^{4+} and Ce^{4+} in oxides.

Crystal	Coordination	Band positions (nm)		References
		Ce^{4+}	Tb^{4+}	
Sr_2ZrO_4	VI	310	400, 345	14
Ba_2ZrO_4	VI	300	400, 350	14
$SrZrO_3$	VI		400, 345	14
$BaZrO_3$	VI	310	400, 340	14
$BaCeO_3$	VI		400	14
$BaHfO_3$	VI		400, 335	14
$BaThO_3$	VI	310	420, 345	14
ZrO_2	VII	280	350	15
$ZrSiO_4$	VIII	315	420, 345	14
$ZrGeO_4$	VIII	315	460, 435, 345	14
$ThGeO_4$	VIII	325		14
ThO_2	VIII		500, 435, 329	14
$Ca_3Ga_2Ge_3O_{12}$	VIII		400	16
$Tb_{2.8}Sc_{2.2}Al_3O_{12}$ (ox.)	VIII		440	13
Phosphate glass		250–270	360–380	12
Sodium silicate glass		240	326	17 and 18
Aluminosilicate glass			420	19
Calcium aluminate glass			350	20

additional possibility of formation of Tb^{4+} ions and color centers related to this tetravalent ion. Indeed, Bezmaternykh *et al.* reported that addition of CaO flux to the melt results in TGG crystals with red-brown coloration due to Ca^{2+}/Tb^{4+} charge compensation.[10] The equilibrium concentration between all these defects can be shifted toward oxygen-vacancy-type defects by reduction and toward Tb^{4+}-type centers by oxidation treatments. One well-known consequence of Ca doping is that electric conduction becomes *p* type because some of the defects act as acceptors.[11] In view of optical applications the second consequence is more detrimental. There is an increase in absorption because as a rule these defects have absorption bands in the near ultraviolet and even in the visible. In the case of Tb^{4+} broad charge transfer (CT) transitions ($Tb^{4+}+O^{2-} \rightarrow Tb^{3+}+O^-$) were reported for many oxides (Table IV). Being allowed transitions, CT transitions are usually quite strong and have typical bandwidths of $1-1.5$ eV.[12] A notable exception is the width of the CT band in terbium scandium aluminum garnet that is only about 0.3 eV.[13] Table IV lists quite a large number of oxygen host materials that exhibit CT transitions of Tb^{4+} with absorption in the visible. Despite different structures and oxygen coordination, the position of the CT band varies only little in the range $400-430$ nm.

Since the samples that we investigated were produced for application as optical isolators, the heavy coloration by the above centers has to be reduced. That is where the idea of doping with cerium came in, as it can provide charge compensation, too. Ce^{4+} has the electronic configuration of xenon, so that electronic transitions do not exist in the visible or near UV. Furthermore, in comparison with Tb^{4+} the CT transitions of Ce^{4+} are appreciably shifted toward higher energy (see Table IV). As they are systematically below

320 nm, they do not handicap any applications in the visible. According to Table IV roughly 0.9 eV more energy is needed to transfer an electron from O^{2-} to Ce^{4+} in comparison to Tb^{4+}. This is an indication for the difference of the Ce^{3+}/Ce^{4+} and Tb^{3+}/Tb^{4+} redox potential which, in a competition between both ions, clearly favors oxidation of cerium.

Hence, the more cerium is added, the more Tb^{4+}, is reduced to Tb^{3+}, thus diminishing its charge-transfer band as well as the bands of more complex centers involving Tb^{4+}. However, there is an optimum where a minimum of absorption is reached, because an excess in cerium doping would result in the presence of Ce^{3+} ions that exhibit again absorption in the visible and near-ultraviolet range. For $Y_3Al_5O_{12}$ all five $4f^1 \rightarrow 5d^1$ transitions are known: 457 nm, 340 nm, 258 nm, 226 nm, and 209 nm.[21] We are here particularly interested in the lowest transition in garnets that occur at 432 nm ($Y_3Ga_5O_{12}$), 433 nm ($Y_3Al_2Ga_3O_{12}$), 437 nm ($Y_3Ga_2Al_3O_{12}$), 445 nm ($Y_3Al_4GaO_{12}$), 448 nm ($Lu_3Al_5O_{12}$), 455 nm ($Gd_3Sc_2Al_3O_{12}$), 459 nm $Y_2GdAl_5O_{12}$, and 469 nm ($Gd_3Al_5O_{12}$).[22] As the $4f$ levels are practically independent from the host material, the observed spread of the positions of the transitions is caused by the stronger crystal field interaction of the $5d$ electrons. Nevertheless, the variation for the lowest $5d$ transition is limited between 430 nm and 470 nm for different garnets, and we assume that the lowest transition of Ce^{3+} in TGG can be expected to be in the same range. This fact complicates the identification of bands for our samples, because the broad electronic Ce^{3+} transition from $4f^1F_{5/2}^2$ ground state to its lowest $5d$ level overlaps with the broad charge-transfer transition of Tb^{4+}. So we may sketch the scenario of doping Ce into TGG:Ca as follows: With increasing cerium content absorption in the

violet is at first diminished by reduction of Tb^{4+}. In samples grown under reducing conditions somewhat earlier, in oxidized samples somewhat later, cerium is going to be built in as Ce^{3+} and not anymore as Ce^{4+}, thus increasing absorption in the violet again by electronic transitions. In general, absorption in the range 400–450 nm therefore is composed of two contributions of quite different physical origin. Assuming that our samples were grown under oxidizing conditions, then we may conclude from Table I that even in the most Ce-rich sample T6 the Ca concentration expressed in mol % is prevailing over the Ce concentration, i.e., even sample T6 is not overcompensated. This is consistent with the above statement that B.42 is smallest for the sample with the highest cerium concentration at the same calcium content.

As B.42 has an associated ODMR spectrum (Reyher *et al.*[6]), the corresponding defect center has to be paramagnetic. Besides Ce^{3+} (Ce^{4+} is not paramagnetic) oxygen vacancies with one trapped electron (F^+ center) and Tb^{4+} ions are possible candidates. Tb^{4+} is an f^7 ion with an $^8S_{7/2}$ state and an important admixtures from higher energy states which might lead to EPR signals with strongly varying effective g factors depending on the ligand fields and the microwave frequency used (see e.g.,[23–26]), so there is a fair chance that one of the ODMR signals for the 420 nm band observed by Reyher *et al.* may also be attributed to Tb^{4+}. In their ODMR spectra (Fig. 2 in Ref. 6) we identify three features. There are two overlapping bands at low magnetic fields, from which the smaller one can only be recognized as a shoulder, and one component at high field. The approximate positions at 70 GHz correspond to 0.8 T, 1.0 T, and 2.8 T, respectively, and at 36 GHz to 0.4 T, 0.5 T, and 1.5 T, respectively with the approximate (effective) g values 6.3, 5.0, and 1.5...1.9, respectively. By comparison with the ODMR tuned to the known Tb^{3+} lines at 489 nm and 377 nm, the peak at $g_{eff} \approx 6.3$ could clearly be identified as one pertinent to the host lattice. The feature with lowest g values were attributed to Ce^{3+}. In that case the values depend much on the site symmetry so that we may regard them as sufficiently supported by investigations of Ce^{3+} in yttrium aluminum garnet where 1.7 and 2.1 was found.[27] Reyher *et al.* attributed the shoulder at $g \approx 5.0$ to an unknown bulk effect, i.e., a terbium-related transition.

MCD, ODMR, as well as tagged MCD from Tb^{4+} ions in the form of an ionized Tb^{3+} ion [designated as $(Tb^{3+})^+$] was studied in phosphate glasses by Bricis *et al.*[28] From ESR studies in different glasses Ebendorff-Heidepriem and Ehrt[29] attribute $g=5.0$ to Tb^{4+}. We therefore infer that the feature with $g \approx 5.0$ in the ODMR spectra of Reyher *et al.*[6] is the one that has to be attributed to the Tb^{4+} ions in our samples, because sample T5.2 of this work is from the same batch as sample S1 in the work of Reyher *et al.* Assuming in addition that the optical Tb^{4+} CT transition and the Ce^{3+} f-d transition practically coincide, the broad magnetic field range of the absorption peak at 420 nm in the tagged MCD spectra becomes understandable, too.

So far, arguments have been presented that clarify the role and interaction of the dopants Ca and Ce with the terbium of the TGG host. In addition, arguments can be found in the literature that link photochromism in the violet range to the presence of Tb^{4+}. Kostyk *et al.* observed the appearance of a photochromic band at 400 nm in Tb-doped calcium-gallium-aluminum garnet after irradiation with UV light that correlates with the Tb concentration and relate it to a radiation-induced $Tb^{3+} \rightarrow Tb^{4+}$ charge exchange.[16] Irradiating terbium-doped silica fibers at about 488 nm produced a broad photoinduced absorption peaking at 420 nm. This photochromic band was found to be stable at room temperature and was related to Tb^{4+}.[30] Investigating terbium-doped aluminasilicates Gerasimova *et al.* observed a radiation-induced photochromic band at 420 nm with a half-width of 0.8 eV and an oscillator strength of 10^{-4} that they attribute to Tb^{4+}.[19] One of their arguments is that the Tb^{3+} bands at 483 nm ($^7F_6 \rightarrow ^5D_4$) and 379 nm ($^7F_6 \rightarrow ^5D_3$) decrease proportional to the increase of the band at 420 nm upon photobleaching by irradiation at 337 nm. In view of these facts, one might wonder whether the broad photoinduced band at 420 nm that can be generated by UV irradiation in Tb-doped gadolinium gallium garnet[31] should likewise be attributed to Tb^{4+} CT bands. In all the above examples the photochromism is related to terbium but in samples that contain no cerium at all. This makes it highly probable that Tb^{4+} is responsible for photochromism in TGG but poses the question whether the cerium doping has anything to do with this photochromism apart from the fact that it acts as a reducing agent and thus diminishes the Tb^{4+} content.

Though still not thoroughly investigated, preliminary results shown in Fig. 3 indicate some dependence on the polarization direction of the pumping light. This might point to a lower symmetry than normal for Tb^{4+} sites which should be attributed to the presence of nearby dopant ions. The excellent fit obtained by using Eq. (1) for the thermal and radiative coloration process [Figs. 8(b) and 2(a), respectively] points to relaxation of the bimolecular reaction type, e.g., by double hole trapping. The exponential behavior found for bleaching must then be attributed to some different process.

In order to explain the above findings in view of the photochromic band B.42 we consider now two models, one in which Ce plays an active role in the photochromism and another one for which we disclaim any contribution of Ce apart from its role in the redox reaction.

In the first model we follow the line suggested in Ref. 32, that pairs with conjugate electron configuration are more stable. This means that if both Ce^{4+} and Tb^{4+} are present in a crystal, then there is a tendency to form stable Ce^{4+}–Tb^{4+} pairs, i.e., the Tb^{4+} "hops" by hole emission and capture until it finds a Ce^{4+} partner, presumably next to a locally negatively charged Ca^{2+} on Ga^{3+} site (all on adjacent or nearby cation sites). Then the photochromic reaction may be regarded as emission and capture of two holes at this complex according to

$$Tb^{4+} + Ce^{4+} \rightleftharpoons Tb^{3+} + Ce^{3+} + 2h. \qquad (2)$$

The complex on the left-hand side is expected to exhibit the special charge-transfer band B.42 that implies here complete decay of the stable tetravalent pair state. The holes, originally introduced by Ca codoping, normally form hole polarons in the oxygen sublattice of most oxides ($O^{2-}+h \rightarrow O^- +$ lattice distortion). In the presence of a Ce surplus, which reduces the number of available holes per Ce and thus

prefers the Ce^{3+} state compared to Ce^{4+}, we in fact observe smaller B.42 bands. For similar reasons of charge compensation we also assume that a nearby Ca^{2+} is needed to stabilize the $Ce^{4+}-Tb^{4+}$ pair.

In our case illumination in the region 476–633 nm was found to result in similar kinetics as at elevated temperatures, which indicates that both the photons and high temperature are needed to overcome some potential barrier. Whether the activation energy of the order of 1 eV found should be attributed to the mobility of hole polarons or to some local excitation remains an open question.

Now let N_0 be the number of ground states destroyed by previous irradiation at $\lambda_p = 458$ nm. Then the temporal increase of the band B.42 by heating-or radiation-assisted mobilization of polarons results from the following kinetics:

$$\frac{dN_G}{dt} = \frac{\beta}{N_0} p^2. \qquad (3)$$

Here N_G is the number of originally destroyed ground states that have been regenerated by capture of two holes, β represents the (initial) recombination rate, and $p = 2(N_0 - N_G)$ is the concentration of available polarons. In this case the transfer of the metastable state (MS) to the ground state (GS) takes place via a pair of charge carriers. The solution of this differential equation is

$$N_G(t) = \frac{N_0}{1 + (4t\beta)^{-1}}, \qquad (4)$$

which is of the same type as Eq. (1), with $\Delta A(t) \propto N_G$, $\Delta A_\infty \propto N_0$, and $1/4\beta = \tau$. This model is supported by the results shown in Figs. 8(b) and 2(a) where the data are described quite well by Eq. (4), viz. (1).

The transfer GS→MS might be described by a charge transfer of the type $h_2 \rightarrow 2h$, so that the temporal evolution of the number of occupied centers in the metastable state is given by an exponential function. This explains the exponential behavior for the decrease of the band B.42 due to light irradiation with 458 nm [Fig. 2(b)].

The bands B.31, B.36, and B.49 are expected to be related to the species showing up on the right-hand side of Eq. (2), possibly also including trapped-hole centers subsequently formed. A good candidate for B.36 and B.49 would be the $4f$-$4d$ transitions of the Ce^{3+} centers. However, a clear assignment requires additional investigations.

We now discuss an alternative model without involvement of cerium. In the simplest case this can be represented by a reaction of the type

$$Tb^{4+} + O^{2-} \rightleftharpoons (Tb^{4+})^- + O^-, \qquad (5)$$
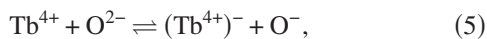
the metastable state being the complex on the right-hand side. By the notation $(Tb^{4+})^-$ we express that this is an ef-

fective Tb^{3+} site that is negatively charged with respect to the neighborhood. Possibly this prevents escape of a hole from O^- and stabilizes the complex. The kinetics of the thermal/radiation induced relaxation to the ground state is then given by

$$\frac{dN_G}{dt} = \frac{\beta}{N_0} N_- N_+, \qquad (6)$$

where N_- is the concentration of $(Tb^{4+})^-$ and N_+ the concentration of O^-. But since $N_+ = N_- = N_0 - N_G$, the solution

$$N_G(t) = \frac{N_0}{1 + (t\beta)^{-1}} \qquad (7)$$

is again of the type of Eq. (1). In this second model the bands B.31, B.36, and B.49 should be attributed to the charge-transfer transition of the metastable complex and possibly to electronic transitions of the $(Tb^{4+})^-$ ion that definitively sees for its $4f$-$5d$ transitions a crystal field that differs from the one at regular lattice positions.

V. CONCLUSION

From the kinetics and spectroscopic measurements we conclude that the ground (stable) state is the state reached after heating. Irradiation with $\lambda_p = 458$ nm leads to a transfer from the ground to the metastable state. The existence of this metastable electronic state is the origin of the observed photochromic (and photorefractive) effect in TGG. The analysis of the measurements and a comparison with literature data of similar systems leads to the conclusion that the ground state is formed by Tb^{4+} or a complex involving Tb^{4+} and that the absorption band at 420 nm is the pertinent charge-transfer band. We proposed two models which both give a possible valid explanation of the kinetics for the "bimolecular" reaction type of thermal/radiative relaxation. More investigations are needed to clarify the role of the redox state and the question of whether cerium plays any role at all for the photochromism in TGG.

*URL: http://nlp.exp.univie.ac.at

[1] A. B. Villaverde, D. A. Donatti, and D. G. Bozinis, J. Phys. C **11**, L495 (1978).

[2] U. V. Valiev, T. V. Virovets, R. Z. Levitin, K. M. Mukimov, B. Y. Sokolov, and M. M. Turganov, Opt. Spectrosc. **57**, 461 (1984).

[3] E. A. Khazanov, O. V. Kulagin, S. Yoshida, D. B. Tanner, and D. H. Reitze, IEEE J. Quantum Electron. **35**, 1116 (1999).

[4] P. K. Tien, R. J. Martin, S. L. Blank, S. H. Wemple, and L. J. Varnerin, Appl. Phys. Lett. **21**, 207 (1972).

[5] B. Sugg, H. Nürge, B. Faust, E. Ruža, R. Niehüser, H. J. Reyher, R. A. Rupp, and L. Ackermann, Opt. Mater. **4**, 343 (1995).

[6] H. J. Reyher, B. Faust, B. Sugg, R. Rupp, and L. Ackermann, J. Phys.: Condens. Matter **9**, 9065 (1997).

[7] G. J. Pogatshnik, L. S. Cain, Y. Chen, and B. D. Evans, Phys. Rev. B **43**, 1787 (1991).

[8] A. Matkovskii, P. Potera, D. Sugak, L. Grigorjeva, D. Millers, V. Pankratov, and A. Suchocki, Cryst. Res. Technol. **39**, 788 (2004).

[9] K. Ohno, T. Abe, and T. Kusunoki, Jpn. J. Appl. Phys., Part 1 **29**, 103 (1990).

[10] L. N. Bezmaternykh, I. A. Gudim, and V. L. Temerov, Rus. J. Surf. Investigation **5**, 20 (2002).

[11] E. Hartmann, L. Kovács, and J. Paitz, Phys. Status Solidi A **86**, 401 (1984).

[12] H. Ebendorff-Heidepriem and D. Ehrt, Opt. Mater. **15**, 7 (2000).

[13] Y. Kagamitani, D. A. Pawlak, H. Sato, A. Yoshikawa, H. Machida, and T. Fukuda, Jpn. J. Appl. Phys., Part 1 **41**, 6020 (2002).

[14] H. E. Hoefdraad, J. Inorg. Nucl. Chem. **37**, 1917 (1975).

[15] N. Van Vugt, T. Wigmans, and G. Blasse, J. Inorg. Nucl. Chem. **35**, 2601 (1973).

[16] L. V. Kostyk, A. E. Nosenko, and V. V. Kravchishin, Opt. Spectrosc. **82**, 548 (1997).

[17] V. I. Arbuzov, V. Y. Grabovskis, and Y. Y. Dzenis, Sov. J. Glass Phys. Chem. **18**, 178 (1992).

[18] J. S. Stroud, J. Chem. Phys. **35**, 844 (1961).

[19] V. I. Gerasimova, Y. S. Zavorotnyi, A. O. Rybaltovskii, and P. V. Chernov, Glass Phys. Chem. **25**, 61 (1999).

[20] H. Hosono, T. Kinoshita, H. Kawazoe, M. Yamazaki, Y. Yamamoto, and N. Sawanobori, J. Phys.: Condens. Matter **10**, 9541 (1998).

[21] T. Tomiki, H. Akamine, M. Gushiken, Y. Kinjoh, M. Miyazato, T. Miyazato, N. Toyokawa, M. Hiraoka, and N. Hirata, Y. Ganaha *et al.*, J. Phys. Soc. Jpn. **60**, 2437 (1991).

[22] P. Dorenbos, J. Lumin. **91**, 155 (2000).

[23] A. Abragam and B. Bleany, *Electron Paramagnetic Resonance of Transition Ions* (Clarendon Press, Oxford, 1970).

[24] S. Hansen, B. D. Mosel, W. Müller-Warmuth, and P. Fielding, Z. Naturforsch., A: Phys. Sci. **51**, 885 (1996).

[25] H. Ebendorff-Heidepriem and D. Ehrt, J. Phys.: Condens. Matter **11**, 7627 (1999).

[26] J. Baker, J. Chadwick, G. Garton, and J. Hurrell, Proc. R. Soc. London, Ser. A **286**, 352 (1965).

[27] H.-J. Reyher, N. Hausfeld, M. Pape, J. Baur, and J. Schneider, Solid State Commun. **110**, 345 (1999).

[28] D. Bricis, J. Ozols, U. Rogulis, J. Trokss, W. Meise, and J. Spaeth, Solid State Commun. **81**, 745 (1992).

[29] H. Ebendorff-Heidepriem and D. Ehrt, Opt. Mater. **18**, 419 (2002).

[30] P. Xie, Electron. Lett. **30**, 1970 (1994).

[31] R. Metselaar, J. P. M. Damen, P. K. Larsen, and M. A. H. Huyberts, Phys. Status Solidi A **34**, 665 (1976).

[32] Y. Wu and C. Shi, Solid State Commun. **95**, 319 (1995).